NJC

New Journal of Chemistry

A journal for new directions in chemistry

Accepted Manuscript

This article can be cited before page numbers have been issued, to do this please use: A. Shaikh, M. Ghosh, P. Mukherjee, A. Ghosh, R. A. Molla, S. Ta and D. Das, *New J. Chem.*, 2020, DOI: 10.1039/D0NJ02415E.

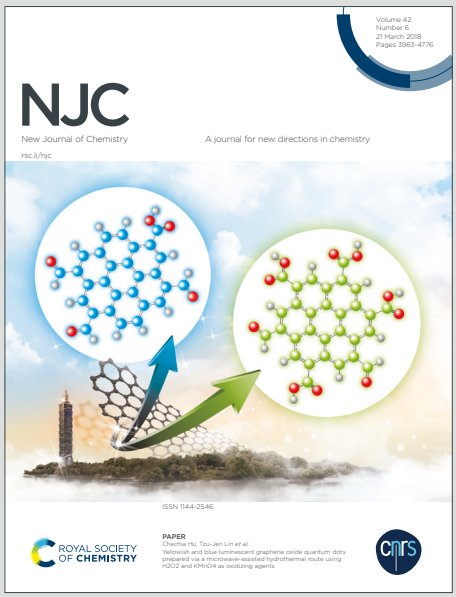

ROYAL SOCIETY OF CHEMISTRY

rsc.li/njc

Journal Name

ROYAL SOCIETY OF CHEMISTRY
View Article Online
DOI: 10.1039/D0NJ02415E

ARTICLE

Amide-imine conjugate involving gallic acid and naphthalene for nano-molar detection, enrichment and cancer cell imaging of La^{3+}: Studies on catalytic activity of La^{3+} complex

4Received 00th January 20xx,
Accepted 00th January 20xx

DOI: 10.1039/x0xx00000x

www.rsc.org/

Ahad Shaikh,[a] Milan Ghosh,[a] Pallabi Mukherjee[a], Avijit Ghosh,[b] Rostam Ali Molla,[c] Sabyasachi Ta*[a] and Debasis Das*[a]

[a]Department of Chemistry, The University of Burdwan, Burdwan, 713104, W.B., India

[b]Centre for Research in Nanoscience & Nanotechnology, (CRNN), University of Calcutta, Technology Campus, Sector-III, Block-JD 2, Salt Lake, Kolkata, 700098, West Bengal, India.

[c]Department of Science and Humanities, S. N. Bose Govt. Polytechnic College, Ratua, Malda, 73213, India

Abstract

Single crystal X-ray structurally characterized amide-imine conjugate (**GAN**), derived from gallic acid and naphthalene selectively recognizes La^{3+} ion via TURN ON fluorescence through ESIPT and CHEF mechanism. The **GAN** can detect as low as 23.93×10^{-9} M La^{3+} ion and image intracellular La^{3+} ion in live HeLa and SiHa cells under fluorescence microscope in a time- and concentration dependent manner. The corresponding [**La(III)-GAN]** complex is established as an efficient catalyst for the synthesis of benzimidazole derivative from *o*-phenylenediamine and substituted benzaldehyde. Moreover, **GAN** is very useful for enrichment of La^{3+} in ethyl acetate medium.

Introduction

Lanthanum (La), a rare earth element is extensively used in industries as a mischmetal alloy in "flints", anode in nickel hydride batteries, to manufacture special optical glasses, carbon lighting in studio, catalyst in petroleum refining etc. In medicinal field, La is used as biological tracer of Ca^{2+}. The radioactive La is used in cancer treatment.[1] Lanthanum carbonate, Fosrenol depresses high blood phosphate levels, known as hyperphosphatemia in human to reduce heart disease and strokes. It is also useful during dialysis of kidney disease.[2-3] Thus, determination of trace amount La is demanding. Large ionic radii, Lewis acidity, unoccupied 5d and 6s orbitals and high coordination number make La^{3+} ion ~~an~~ a useful catalyst for several organic trasformation.[4]

On the other hand, gallic acid (G), an important antioxidant[5-6] inhibits pancreatic cholesterol esterase.[7-9] The G, extracted from tea leaf, oak bark, grapes etc.[7-8] is also used in tanning and ink dye. The G and several other polyphenols selectively damage cancer cell, leaving normal cell unaffected.[10-17] The G is also a potential anti-inflammatory drug.[11-12] Ester form of G has higher bioavailability over G.[13] The G inhibits the rancidity, produced by lipid peroxidation for use in cosmetics and food packaging materials. The G is chosen because it's three –OH groups may stabilize the designed La^{3+} complex in solution through several hydrogen bonds leading to enhanced rigidity of the system, with strong fluorescence.

As already mentioned, La^{3+} compounds are useful catalyst for several organic transformations[18-19] like direct amidation of esters,[20] highly enantio-selective conjugate addition of thioglycolate to chalconescan,[21] trans-esterification of carboxylic esters,[22] asymmetric Mannich-type reaction etc.[23] The benzimidazole derivative being structurally similar to purine bases and binding constituent of several natural products like vitamin B12 are used as potential drug for antitumor/ anticancer, antibacterial, antifungal, antiviral and anti-HIV.[24-25] One-pot synthesis of 2-substituted benzimidazole derivatives from *o*-phenylenediamine and different aldehydes requires lanthanum chloride as catalyst.[26] However, several issues like solvent, temperature and product yield still remain a major concern.

Optical detection and separation of La^{3+} from other Ln^{3+} ions is an attractive research area. Notably, luminescent La^{3+} complexes are relatively rare.[27] The electronic configuration is probably responsible for non-luminous nature of La^{3+} ion that makes it different from other Ln^{3+} ions. Several fluorescent ligands have been employed to recognize La^{3+} ion. For example, Zhao *et. al.* reported a pyridine quinoxaline derivative (HPDQ) for detection of La^{3+} through red shifted fluorescence enhancement.[28] Ahmed *et. al* reported albendazole (ABZ) based La^{3+} sensor where emission intensity is measured as a function of drug concentration.[29] Sayed and his co-workers reported 5-fluorouracil (5-FU) based La^{3+} sensor[30] having binding constant, 0.364×10^4 M^{-1}.

Efficient separation of La^{3+} from mixture of lanthanides (Ln^{3+}) is challenging and demanding.[31-33] Literature suggest that Tian, *et. al.* used N,N-di-alkyl-diglycolamic acid (HDMDGA) for efficient extraction of lanthanides from concentrated nitric acid medium.[34] Binnemans and co-workers developed methane sulphonic acid and di-(2-ethylhexyl)phosphoric acid based organic extractant that separate La^{3+} from terbium-rich lamp phosphor waste.[35] Yin *et. al.* used a low cost chelator, H3cit with P204 for separation of La^{3+} from other Ln^{3+} ions.[36] Bieke *et.al.* have reported extraction of La^{3+} ion using ammonium and phosphonium nitrate system.[37]

These facts inspired us to develop a new probe for trace level selective optical recognition and determination of La^{3+} ion. Herein, single crystal X-ray structurally characterized amide-imine conjugate (**GAN**), derived from gallic acid and 2-hydroxy napthaldehyde is explored for trace level selective recognition of La^{3+} ion in live cells.

Besides, the new [**La(III)-GAN]** complex is exploited as an efficient catalyst for synthesis of benzimidazole derivative by coupling *o*-phenylenediamine and substituted benzaldehyde at room temperature. In addition, **GAN** is useful for enrichment of La^{3+} from mixture of lanthanides (Ln).

Experimental

Synthesis (Scheme 1)

3, 4, 5 –Trihydroxybenzohydrazide (GA)

Excess thionyl chloride is added to the 3, 4, 5-trihydroxybenzoic acid (133 mg, ~1 mmol) under stirring condition and resulting solution is refluxed for 6h. The solid obtained after removal of solvent is purified by solvent extraction using ethyl acetate. The solid isolated after removal of ethyl acetate is refluxed with excess hydrazine for 5h. Finally, removal of solvent yielded solid GA.

(E)-3, 4, 5-Trihydroxy-N'-((2-hydroxynaphthalen-1-yl)methylene)benzohydrazide (GAN)

The mixture of GA (133 mg, 1 mmol) and 2-hydroxynapthaldehyde (172 mg, 1 mmol) in methanol is refluxed for 6h to obtain wine color solution which upon slow evaporation produces needle shape red crystals, suitable for single crystal X-ray diffraction (SC-XRD) analysis. The yield is 70%. Anal. calcd. (%): C, 63.90; H, 4.17 and N, 8.28; found: C, 63.40; H, 4.82 and N, 8.95. ESI-MS(+), m/z, calcd. for $C_{18}H_{14}N_2O_5$, 338.09; found, 339.09 [**GAN**+H]$^+$ [**Fig. S1, ESI**]. ^{1}HNMR [400 MHz, $CDCl_3$, TMS, J (Hz), δ (ppm)]: 11.41 (1H, s), 9.691 (1H, s), 9.249 (1H, s), 9.03 (1H, s), 6.94- 8.24 (aromatic region), 7.518(1H, s) [**Fig. S2, ESI**].

^{13}CNMR [400 MHz, $CDCl_3$, TMS, J (Hz), δ (ppm)]: 167.85, 161.81, 145.86, 139.11, 135.20, 134.75, 131.83, 129.31, 127.79, 127.56, 123.31, 122.32, 106.83, 106.17, 105.86 and 104.77 [**Fig. S3, ESI**]. FTIR (cm^{-1}), 3446 (NH), 3335.66 (OH), 2981.74 (imine CH), 1608 (C=O) and 1446 (C=N) [**Fig. S4, ESI**].

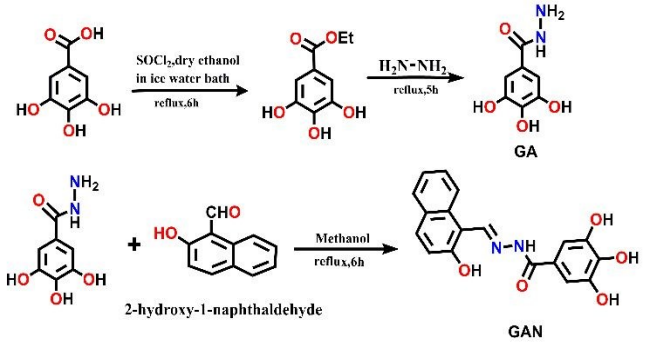

Scheme 1 Synthesis of **GAN**

[La(III)-GAN] complex

To a magnetically stirred acetonitrile solution of **GAN**, methanol solution of $La(NO_3)_6.6H_2O$ is added drop-wise. After stirring for 40-45 min, the solution is filtered. The filtrate is kept for slow evaporation whereby yellow solid is collected after 5 days. The ESI-MS(+), m/z calcd. for $C_{18}H_{13}LaN_5O_4$, [**La(III)-GAN**+H]$^+$ 663.23. Found : 663.45; [**La(III)-GAN**+Na+H_2O]$^+$, 703.23; found: 702.70; [**La(III)-GAN**+2H_2O+C_2H_5OH]$^+$, 744.33, found: 743.72; [GA+2LiCl+H]$^+$, 269.94; found: 269.93 **[Fig. S5, ESI]**. FTIR (cm^{-1}), 3426 (OH), 1636 (C=O), 1457 (C=N) **[Fig.S6, ESI]**.

[La(III)-GAN] complex catalyzed synthesis of benzimidazole derivative

In general, 1.0 mmol of *o*-phenylenediamine is added to the ethanol solution of the substituted aldehyde (1.0 mmol, 5.0 mL) in presence of 10 mg catalyst. The reaction mixture is stirred at room temperature while the progress is monitored by thin layer chromatography (TLC). After 45 min, the solid product isolated by filtration is purified by crystallization from ethanol.

Single crystal X-ray diffraction studies

The ortep view of **GAN** is presented in **Fig. 1**. Intermolecular hydrogen bond contributes to the packing of **GAN** units *via* –OH group having $P2_1/n$ space group. The crystallographic data and refinement details are collected in **Table S1 [ESI].** Selected bond lengths and angles are listed in **Table S2 [ESI]**.

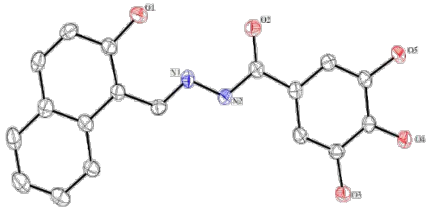

Fig. 1 ORTEP view of **GAN** (50% thermal ellipsoid probability)

Result and discussion

Spectroscopic studies

As **GAN** have pH-sensitive hydroxyl group, the effect of pH on its emission characteristics in presence and absence of La^{3+} is thoroughly investigated and presented in **Fig. S7 [ESI]**. Thus, **GAN** and La^{3+} are mixed in different sets at different pH from pH 3.0 - 12.0 and their emission profile is monitored. **Fig. S7 [ESI]** the optimum performance of **GAN** is observed near physiological pH, 7.4 that allow to carry out the entire studies at pH 7.4 using HEPES buffered aqueous DMSO (DMSO/ H_2O, 4/1, v/v, 10 mM HEPES buffer) media. Interestingly, optimum performance is observed in 20% aqueous DMSO (v/v) media.

The interaction of the **GAN** with La^{3+} is monitored by different spectroscopic techniques. The steady state emission of **GAN** is perturbed by La^{3+} at nano-molar level while other tested common cations *viz.* Ce^{4+}, Pr^{3+}, Nd^{3+}, Sm^{3+}, Eu^{3+}, Gd^{3+}, Tb^{3+}, Dy^{3+}, Ho^{3+}, Er^{3+}, Yb^{3+}, Lu^{3+}, Fe^{3+}, Fe^{2+}, VO^{2+}, Cr^{3+}, Mn^{2+}, Co^{2+}, Ni^{2+}, Cu^{2+}, Zn^{2+}, Hg^{2+}, Pb^{2+} and Cd^{2+} remain reluctant (λ_{ex}, 336 nm)**[Fig. S8, ESI]**. The effect of tested cations on the UV light irradiated bare eye view of **GAN** indicates that La^{3+} turns colourless **GAN** to bright green [**Fig. S9, ESI]** while other cations remain spectator.

The competitive experiment in presence of common cations indicates no significant interference during **GAN** assisted La^{3+} sensing (**Fig. S10, ESI)**.

The weak emission of **GAN** at 396 nm (λ_{ex} = 336 nm) experiences red shift in presence of La^{3+} to 472 nm resulting green emission **[Fig. S11, ESI]**. The intensity of green emission gradually increases upon gradual addition of La^{3+} (**Fig. 2a**) to maximum 97 fold with an isobestic point at 435 nm. Moreover, the plot of emission intensity *vs.* La^{3+} concentration follows a sigmoidal pattern **[Fig. S12, ESI]**, the linear region of which is useful for determination of unknown La^{3+} concentration **[Fig. S13, ESI]**. It is noteworthy that addition of 75 equiv. or more La^{3+} quenches the fluorescence probably due to static quenching. While mathematically calculated lowest detection limit for La^{3+} is 23.93×10^{-9} M,[38] the practical detection limit is 5.0×10^{-9}M [**Fig. S14, ESI**]. The quantum yields of **GAN** and its La^{3+} complex are 0.016 and 0.321 respectively.

The absorption spectrum of **GAN** exhibits peaks at 325 nm (ε = 7.5×104 M^{-1} cm^{-1}) and 361 nm (ε =5.5×103 M^{-1} cm^{-1}), assigned to π–π* and n-π* electronic transitions respectively. Gradual addition of La^{3+} weakens both the peaks gradually along with the appearance of a new band at 412 nm through an isobestic point at 387 nm (**Fig. 2b**).

The Job's plot[39] derived from fluorescence titration data indicates 1:1 (mole ratio) interaction between **GAN** and La^{3+} [**Fig. S15, ESI**], also corroborated from ESI-MS mass spectrum of the resulting complex [**Fig. S6, ESI**]. The association constant of **GAN** for La^{3+}, determined from Benesi-Hildebrand plot using fluorescence titration data is 1.1×10^5 M [**Fig. S16, ESI**].

The weak emission of the **GAN** is attributed to the excited state intramolecular proton transfer (ESIPT) involving naphthol proton

and imine nitrogen. Interaction of **GAN** with La^{3+} inhibits the ESIPT process leading to chelation-enhanced fluorescence (CHEF) (**Scheme 2**).

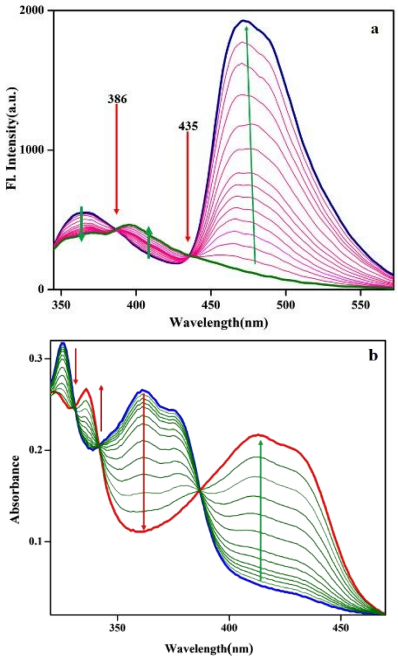

Fig. 2. Changes in the spectra of **GAN** (20 μM) upon addition La^{3+} in DMSO/ H_2O (4 /1, v/v, 10 mM HEPES buffer, pH 7.4; λ_{ex}, 336 nm) [La^{3+}] = 0.001, 0.01, 0.1, 1, 10, 50, 100, 200, 300, 400, 600, 800, 1000, 1200, 1400, 1500, 1800, 2000, 2400 and 3000 μM: (a) emission and (b) absorption

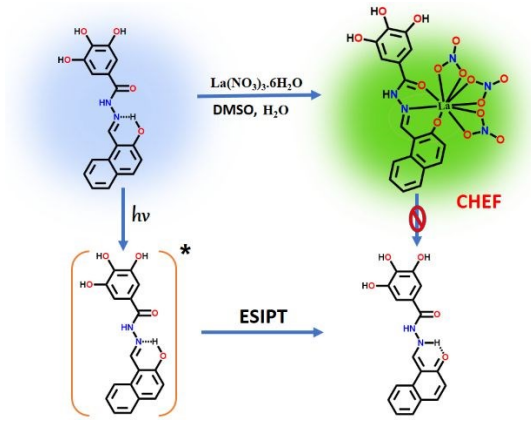

Scheme 2. Probable sensing mechanism

NMR titration

The mode of binding of **GAN** with La^{3+} in solution is established by ^{1}HNMR titration. After addition of 1.0 equiv. La^{3+} to **GAN**, among three types of OH protons (two types from gallic acid and one type from 2-hydroxy-1-napthaldehyde), the most downfield peak at 11.39 ppm (-OH of 2-hydroxy-1-napthaldehyde) disappear along with minor shift of other two type protons (from 9.25 to 9.32 and 9.06 to 9.12). This fact clearly indicates the involvement of phenol-O to the binding of La^{3+}. In addition, imine proton of **GAN** downfield shifted from 9.69 to 9.72 ppm, indicating coordination of imine-N to La^{3+} leading to inhibition of PET process.

The comparison table (**Table S3, ESI**) shows the efficiency of **GAN** for La^{3+} sensing over other pioneering La^{3+} sensors.

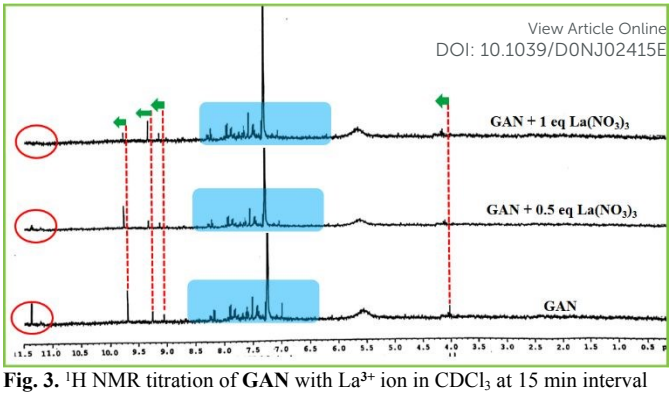

Fig. 3. ^{1}H NMR titration of **GAN** with La^{3+} ion in $CDCl_3$ at 15 min interval

Catalytic activity

Literature on use of La^{3+} complex as catalyst for condensation reaction inspired us to study the catalytic activity of the **[La(III)-GAN]** complex for synthesis of benzamidazole derivative by condensing aromatic aldehyde with *o*-phenylenediamine in ethanol (**Scheme 3**).

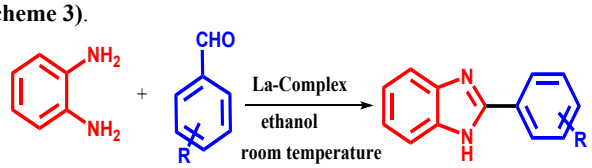

Scheme 3 Synthesis of benzimidazole derivative using **[La(III)-GAN]** complex as catalyst.

Different parameters for this catalytic condensation reaction have been optimized.

Although, 22% yield of the product is observed after 24h reaction in ethanol without catalyst, the reaction time significantly reduces in presence of the catalyst (**Table S4, ESI**). At 10 mg catalyst load, the product yield reaches maximum. The effect of solvent on product yield indicates that polar protic solvent like ethanol and methanol are preferable over polar aprotic solvent like acetonitrile. In fact, the product yield becomes highest in ethanol. Effect of reaction time on the yield of the product indicates a maximum 95% yield after 45 min under optimized reaction conditions.

At optimized reaction conditions, the condensation of *o*-phenylenediamine with different substituted aldehydes lead reasonably good yield of the product at short time **(Table S5, ESI)**.

***In vitro* live cell imaging**

Human cervical cancer HeLa and SiHa cells are cultured in Dulbecco's modified eagle medium (DMEM) supplemented with 10% heat-inactivated fetal bovine serum (FBS) and 1% penicillin/streptomycin at 37°C and 5% CO_2. For *in vitro* imaging studies, the cells are seeded in 12-well tissue culture plates with a seeding density of 10^5 cells per well. After reaching 60%–70% confluence, the previous DMEM medium is replaced with serum-free DMEM medium (colorless), supplemented with 20 μM **GAN** and incubated for 2h to facilitate the probe uptake by cells. Then cells are washed three times with PBS buffer to remove any extracellular **GAN**. Then La^{3+} (50 μM) is added to the medium and further incubated for 1h. The control experiments have been performed by incubating the cell only with **GAN** and La^{3+} separately. After washing with PBS buffer, images of live cells (**Fig 4-5**) are captured using an EVOS® FL cell imaging system, Life Technologies, USA).

No fluorescence is observed in cells that are not previously exposed either to $La(NO_3)_3$ (**Fig. 4e, 5e**) or **GAN** (**Fig. 4b, 5b**). Cells that are exposed to La^{3+} display strong fluorescence in green channel (**Fig. 4h, 4k and 5h, 5k**) and no fluorescence in red channel. Thus, the probe efficiently detects intra-cellular La^{3+} ion in live cell.

View Article Online
DOI: 10.1039/D0NJ02415E

Time and concentration dependent cell imaging studies

For fluorescence visualization of intracellular La^{3+}, HeLa and SiHa cells are incubated with varying concentration of **GAN** (20-100 μM) and La^{3+} (20-100 μM) at 37^{0}C and 5% CO_2 in culture medium. After washing with PBS thrice, the fluorescence images of the cells are captured (**Figs. 6-7**).

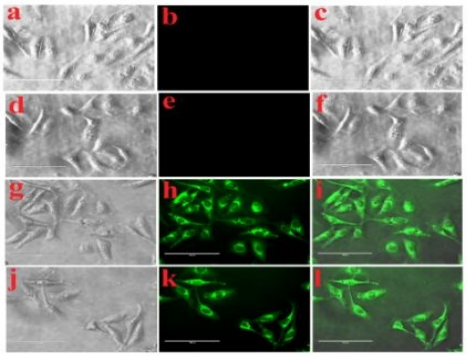

Fig. 4. Imaging of La^{3+} in HeLa cells: (a) bright field image of cells after incubating with **GAN** (20 μM); (b) fluorescence image of the same cells of set (a); (c) overlay images of (a) and (b); (d) bright field image of cells after incubating with La^{3+} (50 μM) only; (e) fluorescence image of the same cells of set (d); (f) merge images of (d) and (e); (g) and (j) are bright field images of cells after incubating with **GAN** (20 μM); (h) and (k) are fluorescence image of the cells in (g) and (j) upon incubation with 50 μM La^{3+}; (i) and (l) are merge images of (g), (h) and (j), (k) respectively (scale bar 200 μm).

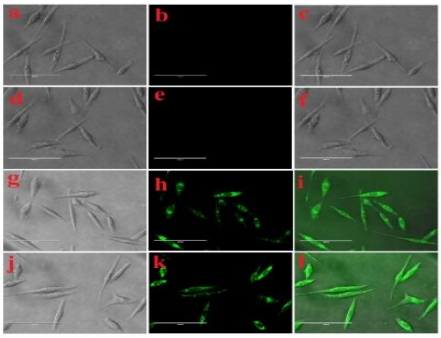

Fig. 5 Imaging of La^{3+} in SiHa cells: (a) bright field image of cells after incubating with **GAN** (20 μM); (b) fluorescence image of the same set of cells; (c) overlay images of (a) and (b); (d) bright field image of cells after incubating with La^{3+} (50 μM) only; (e) fluorescence image of the same set of cells; (f) merge images of (d) and (e); (g) and (j) are bright field images of cells after incubating with **GAN** (20 μM); (h) and (k) are fluorescence image of the cells in (g) and (j) upon incubation with 50 μM La^{3+}; (i) and (l) merge images of (g), (h) and (j), (k) respectively (scale bar 200 μm).

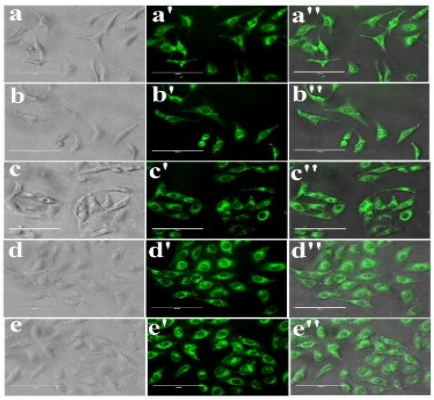

Fig. 6. La^{3+} concentration dependent imaging of **HeLa** cells: (**a-e**) bright field image of cells after incubating with **GAN** (20 μM); (**a'-e'**) fluorescence image of the cells after incubating with different concentration of La^{3+} ranging from 20, 30, 40, 50 and 100 μM respectively and (**a''-e''**) are merged images (bright field and fluorescence) of cells (scale bar 200 μm).

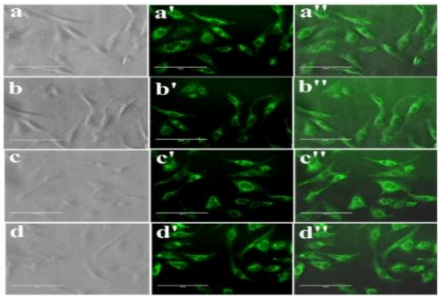

Fig. 7. **GAN** concentration dependent imaging of HeLa cells: (a-d) bright field image of cells after incubating with La^{3+} (50 μM); (a'-d') fluorescence image of the cells after incubating with different concentration of **GAN** ranging from 20, 30, 40, 50 and 100 μM respectively; (a''-d'') merge images (bright field and fluorescence) of cells (scale bar 200 μm).

Moreover, it is observed that with increasing incubation time, the fluorescence intensity in green channel increases. Therefore, a time dependent fluorescence imaging is performed with live SiHa cells and presented in **Fig. 8**.

Thus, cell permeable and stable **GAN** effectively bind intracellular La^{3+} that allow its intracellular imaging. The cytotoxicity of the **GAN** on Hela cells have been tested by MTT assay (**Fig.S17, ESI**). It is observed that 90% of the cells upon treatment with 20 μM of **GAN** for 12h remain alive. Hence, the concentration of the **GAN** has been fixed to 20 μM in all cell line experiments.

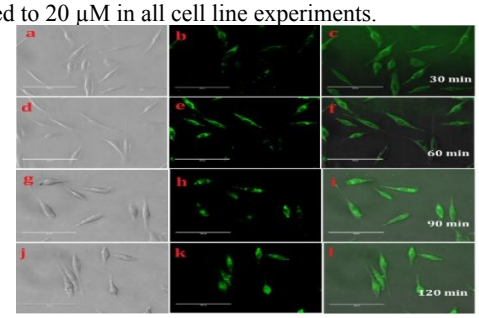

Fig. 8. Incubation time dependent fluorescence images of SiHa cells exposed to 50 μM La^{3+} and 20 μM **GAN**: (a) bright field image of cells after 30 min; (b) fluorescence image of the same set of cells; (c) overlay images of (a) and (b); (d) bright field image of cells after 60 min; (e) fluorescence image of the same set of cells; (f) merge images of (d) and (e); (g) bright field image of cells after 90 min, (h) fluorescence image of the same set cells; (i) overlay images of (g) and (h); (j) bright field images of cells after 120 min; (k) are fluorescence image of the same set cells; ((l) merge images of (j), (k) respectively (scale bar 200 um).

La^{3+} enrichment studies

The selective and quantitative extraction of La^{3+} from aqueous solution to organic solvent is tested with **GAN.** Among different solvents tested for improved efficiency, namely $CH_3COOC_2H_5$ (E%, 98.95), $CHCl_3$ (E%, 98.89), CCl_4 (E%, 98.80) and DCM (E%, 98.69), the extraction efficiency is highest with $CH_3COOC_2H_5$. The extraction efficiency is measured using present method through monitoring of emission intensity of [**La(III)-GAN**] complex in organic phase at 472 nm **(Fig. 9-10).** It is found that the efficiency of La^{3+} extraction using **GAN** is higher than that of gallic acid, ethyl gallate and gallic acid hydrazide (**Table S6, Fig. S18, ESI**). The La^{3+} extraction efficiency of **GAN** is compared with other pioneering extractant available in the literature (**Table S7, ESI).**

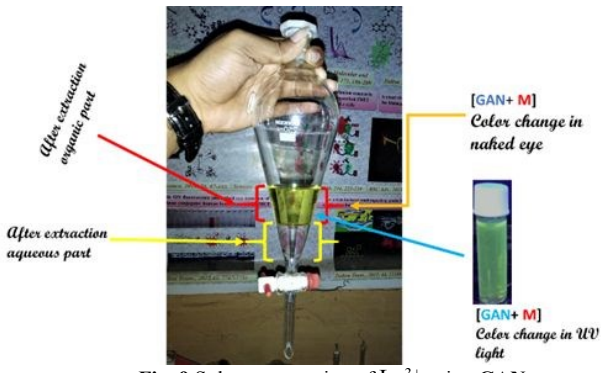

Fig. 9 Solvent extraction of La^{3+} using **GAN**

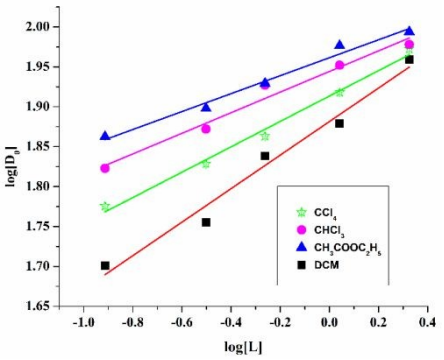

Fig.10. Effect of solvent on La^{3+} extraction

Conclusion

An amide-imine conjugate (**GAN**) derived from gallic acid and naphthalene is structurally characterised by single crystal X-ray diffraction analysis. The **GAN** selectively recognizes La^{3+} ion as low as 23.93×10^{-9}M. La^{3+} triggered CHEF assisted inhibition of ESIPT process is responsible for TURN ON fluorescence of the **GAN**. The **GAN** can image intracellular La^{3+} ion in live HeLa and SiHa cells under fluorescence microscope in a time- and concentration dependent manner. In addition, the [**La(III)-GAN**] complex efficiently catalyses the synthesis of benzimidazole derivative from *o*-phenylenediamine and substituted benzaldehyde. Finally, **GAN** is very useful for enrichment of La^{3+} from aqueous to ethyl acetate medium.

Conflicts of interest

There are no conflicts of interest

Acknowledgement

A. Shaikh acknowledge CSIR, New Delhi for financial assistance. P. Mukherjee acknowledges DST (New Delhi) for Inspire fellowship. We acknowledge the assistance rendered by CAS(II) (UGC) to Department of Chemistry, The University of Burdwan.

Notes and references

CCDC No. of **GAN** is **1889365**. These data can be obtained free of charge *via* http://www.ccdc.cam.ac.uk/conts/retrieving.html or from Cambridge Crystallographic Data Centre, 12 Union Road, Cambridge CB2 1EZ, UK; fax: (+44) 1223-336-033; or e-mail: deposit@ccdc.cam.ac.uk.

1. V. K. Gupta, S. Jain and S. Chandra, Analytica Chimica Acta., 2003, 486, 199–207.
2. M. Pennick, K Dennis and S. J. Damment, J. *Clin. Pharmacol*. 2006, **46**, 738–746.
3. D. M. Weekes, C. F. Ramogida, M. de G. Jaraquemada-Peláez, B. O. Patrick, C. Apte, T. I. Kostelnik, J. F. Cawthray, L. Murphy and C. Orvig, *Inorg. Chem.*, 2016, **55**, 12544–12558.
4. Aillaud, C. Olier, Y. Chapurina, J. Collin, E. Schulz, R. Guillot, J. Hannedouche and A. Trifonov, *Organometallics*, 2011, **30**, 3378–3385.
5. D. O. Kim, K.W. Lee, H. J. Lee and C. Y. Lee, *J Agric Food Chem.*, 2002, **50**, 3713–3717.
6. P. S. M. Prince, M. R. Kumar and C. J. Selvakumari, *J Biochem Molecular Toxicology*, 2010, **25**, 101-107.
7. A. A. Zanwar, S. L. Badole, P. S. Shendek , M. V. Hegde and S. L. Bodhankar, *Polyphenols in Human Health and Disease,* 2014, **1**, 267-271.
8. A. D. Covington. Chem Soc Rev 1997, 26, 11126. *Polyphenols in Human Health and Disease*, **80**, 1045–1047.
9. S. Ngamukote, K. Ma¨kynen, T. Thilawech and S. Adisakwattana, *Molecules*, 2011, **16(6)**, 5054- 5061.
10. E. J. Park and J.M. Pezzuto, *Cancer Metast Rev,* 2002, **21**, 231-55.
11. B. H. Kroes, A.J. van den Berg, H. C. Quarles van Ufford, H. van Dijk, R. P. Labadie, *Planta Med.*, 1992, **58**, 499–504.
12. S. H. Kim, C. D. Jun, K. Suk, B. J. Choi, H. Lim, S. Park, S. H. Lee, H. Y. Shin, D. K. Kim, T. Y. Shin, *Toxicological Sciences*, 2006, **91**, 123–131
13. V. Wacher, L.Z. Bent., US Patent 6, 2001, 180, 666 B1
14. A. K. Mittal, S. Kumar and U. C. Banerjee, *Journal of Colloid and Interface Science*, 2014, **431**, 194-199
15. G. C. Yen, P. D. Duh and H. L. Tsai, *Food Chem.* 2002, **79**, 307-313.
16. T. Green, K. Atkin and U. Macleod, *Br. J. Cancer*, 2015, **112**, S41–S49.
17. V. M. Kulkarni, D. Bodas and K. M. Paknikar, *RSC Adv*., 2015, **5**, 60254-60263.
18. J. Lu, Y. Bai, Z. Wang, B. Yang and H. Ma, *Tetrahedron Letters*, 2000, **41**, 9075–9078.
19. (a) T. Imamoto, Academic Press: New York, 1994. (b) S. Kobayashi, Synlett 1994, **9**, 689-701. (c) G. A. Molander, *Chem. Rev.* 1992, **92(1)**, 29-68.
20. H. Morimoto, R. Fujiwara, Y. Shimizu, K. Morisaki, and T. Ohshima, *Org. Lett*., 2014, **16**, 2018–2021.
21. Y. Hui, J. Jiang, W. Wang, W. Chen, Y. Cai, L. Lin, X. Liu, X. Feng, *Angew. Chem.,* 2010, **49**, 4290 –4293.
22. M. Hatano, Y. Furuya, T. Shimmura, K. Moriyama, S. Kamiya, T. Maki and K. Ishihara, *Org. Lett.,* 2011, **13**, 426–429.
23. H. Morimoto, G. Lu, N. Aoyama, S. Matsunaga and M. Shibasaki, *J. Am. Chem. Soc*., 2007, **129**, 9588–9589.
24. A. Kamal, M. P. Narasimha Rao, P. Swapna, V. Srinivasulu, C. Bagul, A. B. Shaik, K. Mullagiri, J. Kovvuri, V. S. Reddy, K. Vidyasagar and N. Nagesh, *Org. Biomol. Chem*., 2014, **12**, 2370-2387.
25. F. Hoebrecker, *Ber.,* 1872, **5**, 920-926.
26. Y. Venkateswarlu, S.R. Kumar, P. Leelavathi, *Organ. Med. Chem. Lett*., 2013, **3**, 2-8
27. S. Chall, S. S. Mati, S. Rakshit and S. C. Bhattacharya, *J. Phys. Chem. C*, 2013, **117**, 25146-25159.
28. Q. Zhao, X. M. Liu, H. R. Li, Y. H. Zhang and X. H. Bu, *Dalton Trans.*, 2016, **45**, 10836-10841.

View Article Online
DOI: 10.1039/D0NJ02415E

29. A. A. Hamad, R. Ali, H. R. H. Ali, D. M. Nagyc and S. M. Derayea, *RSC Adv.,* 2018, **8**, 5373-5381.
30. N. A. El-Maali, A. Y. Wahman, A. A.M. Aly, A. Y. Nassar and D. M. Sayed, *Appl Organometal Chem.,* 2020; **34**, e5594
31. R. Safarbali, M. R. Yaftian and A. Zamani, *Journal of Rare Earths*, 2016, **34**, 91-98.
32. M. Tian and Q. Jia, *J. Rare Earths*, 2013, **31**, 604-608.
33. H. Hou, Y. Wang, J. Xu and J. Chen, *J. Rare Earths*, 2013, **31**, 1114-1118.
34. Y. Zhang, S. Yang, X. Yuan, Y. Zhao and G. Tian, *Chem. Commun.,* 2017, **53**, 6421- 6423.
35. L. Gijsemans, F. Forte, B. Onghena and K. Binnemans, *RSC Adv.*, 2018, **8**, 26349-26355.
36. S. Yin, W. Wu, X. Bian, Y. Luo and F. Zhang, *Int. J Nonferrous Metal.*, 2013, **2**, 75-79.
37. B. Onghena, E. Papagni, E. R. Souza, D. Banerjee, K. Binnemans and T. V. Hoogerstraete, *RSC Adv.*, 2018, **8**, 32044-32054.
38. M. Ghosh, D. A. Ghosh, S. Ta, J. S. Matalobos and D. Das, *Chemistry Select*, 2017, **2**, 7426-7431.
39. B. F. Parker, Z. Zhang, L. Rao and J. Arnol, *Dalton Trans*., 2018, **47**, 639-644.

View Article Online
DOI: 10.1039/D0NJ02415E

Graphical abstract